

Supplementary Materials and Methods

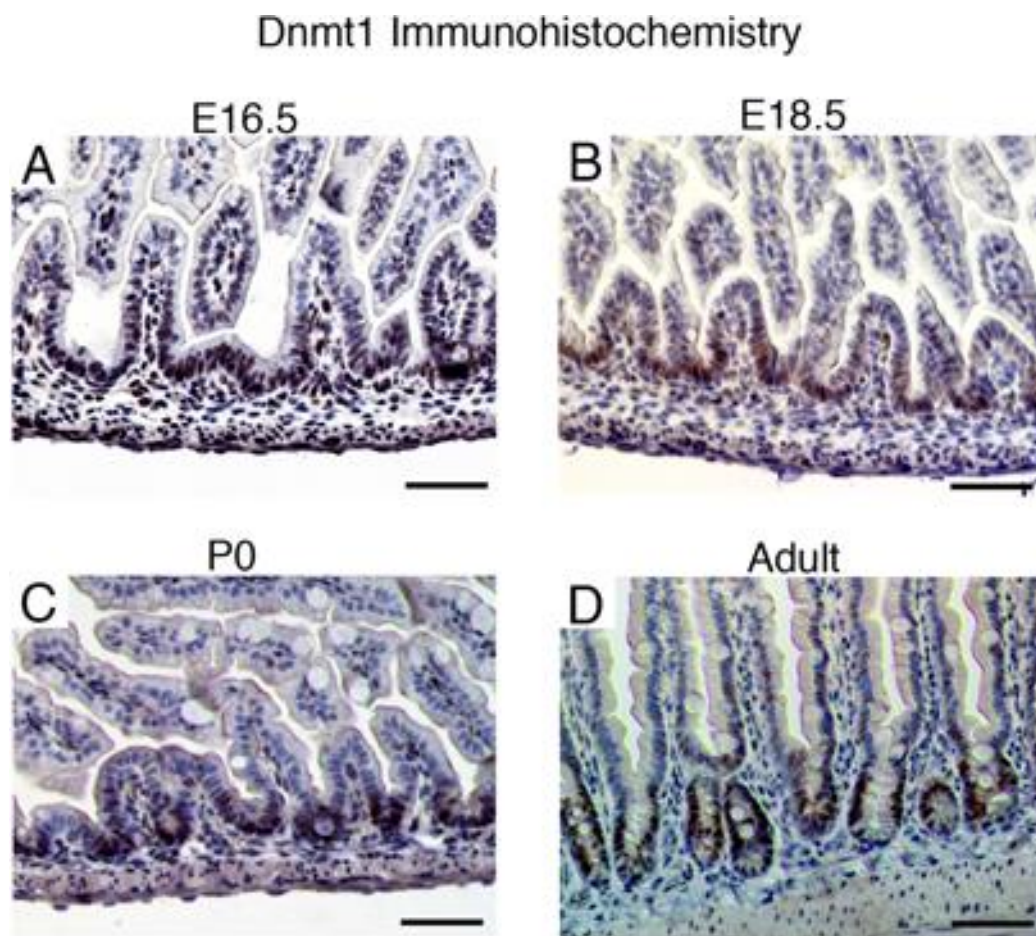
Laser Capture Microdissection for RNA-Seq analysis

For laser-capture microdissection (LCM), proximal jejunum was collected from *Dnmt1^{loxP/loxP}; VillinCre* neonatal litters. Tissue was fixed for one hour in cold methacarn solution (60% methanol, 30% chloroform, 10% glacial acetic acid), washed 3 times in cold 70% ethanol, and submitted for paraffin embedding and sectioning. Serial sections were cut for mutants (*Dnmt1^{loxP/loxP}; VillinCre*, n=2) and controls (*Dnmt1^{loxP/+}*, n=3). Odd numbered sections were mounted onto charged glass slides, and were used for Ki67 IF staining as described above. Ki67 stained sections were scanned using a 10X objective and Metamorph imaging software; scans served as the map for LCM on unstained sections. Even numbered sections were mounted onto non-charged glass slides for use in LCM. The PixCell II LCM system (Arcturus, Applied Biosystems; 7.5- μ m diameter laser spot) was used to capture Ki67⁻ intervillus cells from mutants (n=2) and Ki67⁺ intervillus cells from controls (n=3).

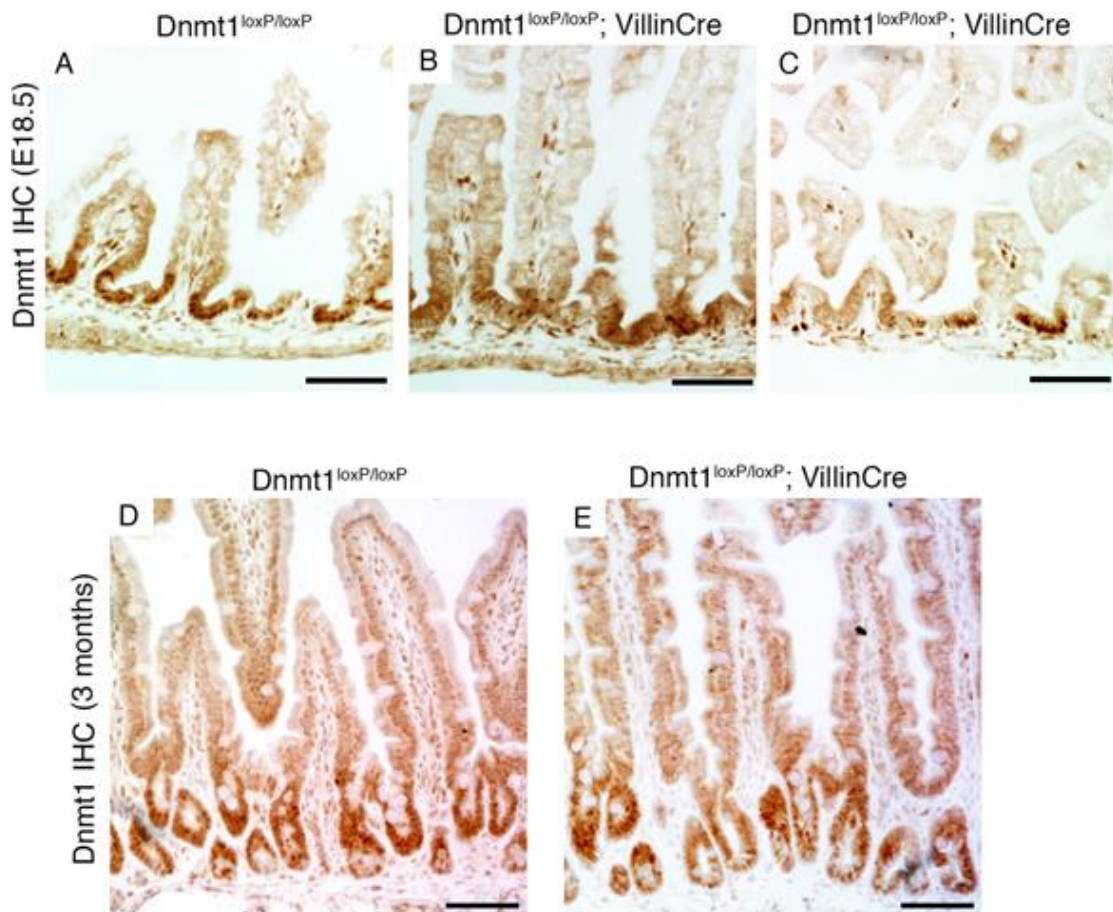
Histology, Immunohistochemistry and Immunofluorescence

Tissues were fixed overnight in 4% paraformaldehyde and subsequently embedded in paraffin. Hematoxylin and eosin staining were used to assess global morphology of intestinal epithelial specimens. Immunohistochemistry staining for Dnmt1 (1:100 Santa Cruz 20701) and Ki67 (1:500 BD Pharmingen 550609) was performed using the ABC detection system (Vector Laboratories). Briefly, following antigen retrieval all slides were blocked with 3% H₂O₂, avidin, and biotin (Vector Laboratories). Additionally, for staining of Dnmt1 slides were blocked for 15 minutes with CAS Block (Invitrogen), and for staining of Ki67 slides were blocked for 2 hours with 5% Normal Donkey Serum (EMD Millipore) in 1%BSA in PBS. All sections were incubated with respective primary antibody at 4°C overnight. The next day,

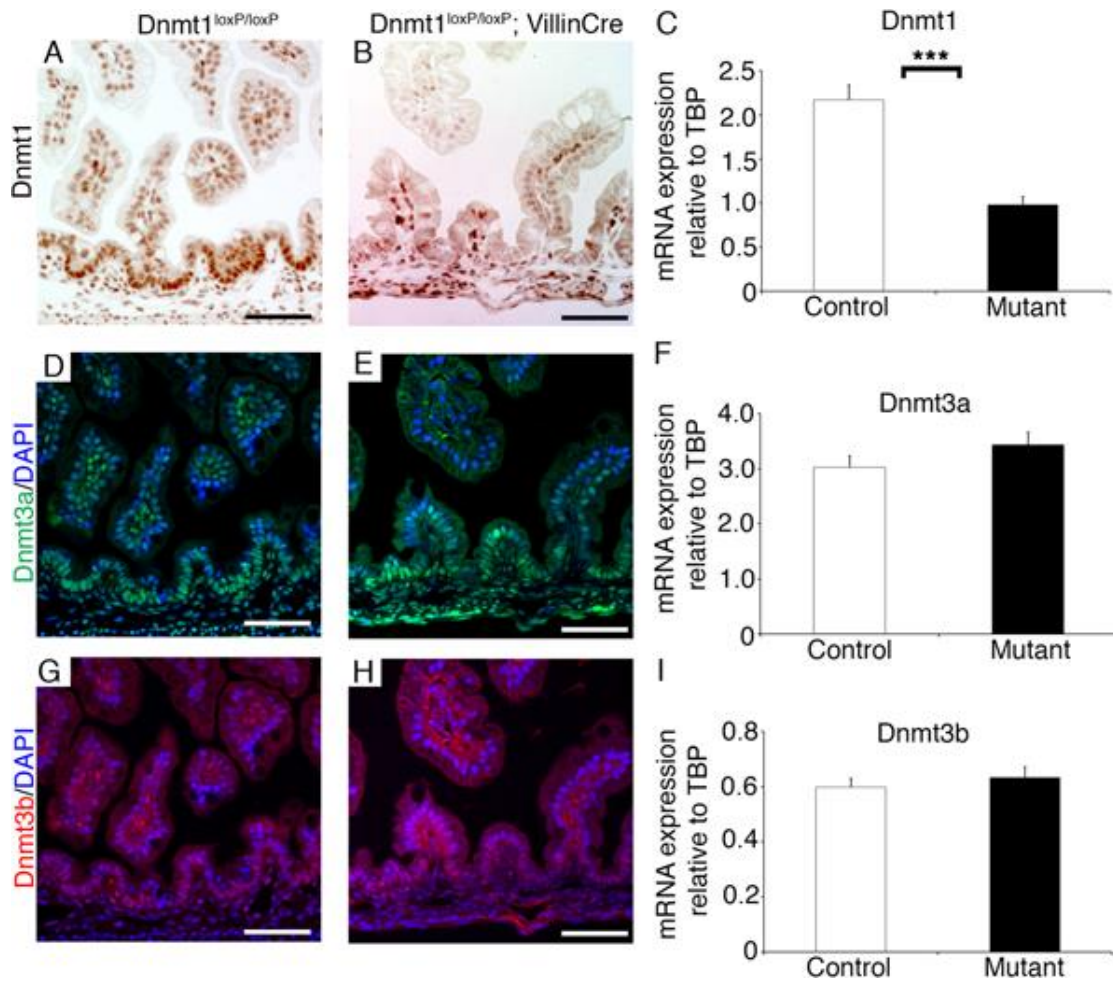
slides were incubated with biotinylated secondary antibody (Vector Laboratories) followed by treatment with ABC reagent, and developed with DAB (Vector Laboratories). p21 immunohistochemistry (1:50 BD Pharmingen 556430) was performed as described previously (van de Wetering et al. 2002). Standard immunofluorescence procedures were performed with the following antibodies: Chromogranin A (1:200 Immunostar 20085), Ki67 (1:500 BD Pharmingen 550609), Dnmt3a (1:500 Santa Cruz 20703), Dnmt3b (1:500 Imgenex 184A), E-cadherin (1:500 BD Transduction Lab 610181), Lysozyme (1:3,000 Dako A0099), Mucin2 (1:50 Santa Cruz 15334), and γ H2AX (1:200 Cell Signaling 2577L). For E-cadherin and γ H2AX staining, tissues were blocked for 15 minutes with CAS Block (Invitrogen). For staining of Chromogranin A, Lysozyme, Mucin2, Dnmt3a, and Dnmt3b, tissues were blocked for 2 hours at room temperature with 5% normal donkey serum (EMD Millipore) in 1% BSA in PBS. All tissues were incubated with respective primary antibody overnight at 4°C. The following day, slides were incubated with immunofluorescent secondary antibodies (The Jackson Laboratory), counterstained with DAPI, and mounted with fluorescence mounting medium. Co-staining was accomplished by sequential IHC and IF antibody staining. Alkaline phosphatase staining was performed using NBT and BCIP (Boehringer). An immunofluorescent TUNEL assay (Boehringer) was used to assess apoptosis. All microscopy was performed on a Nikon Eclipse 80i.



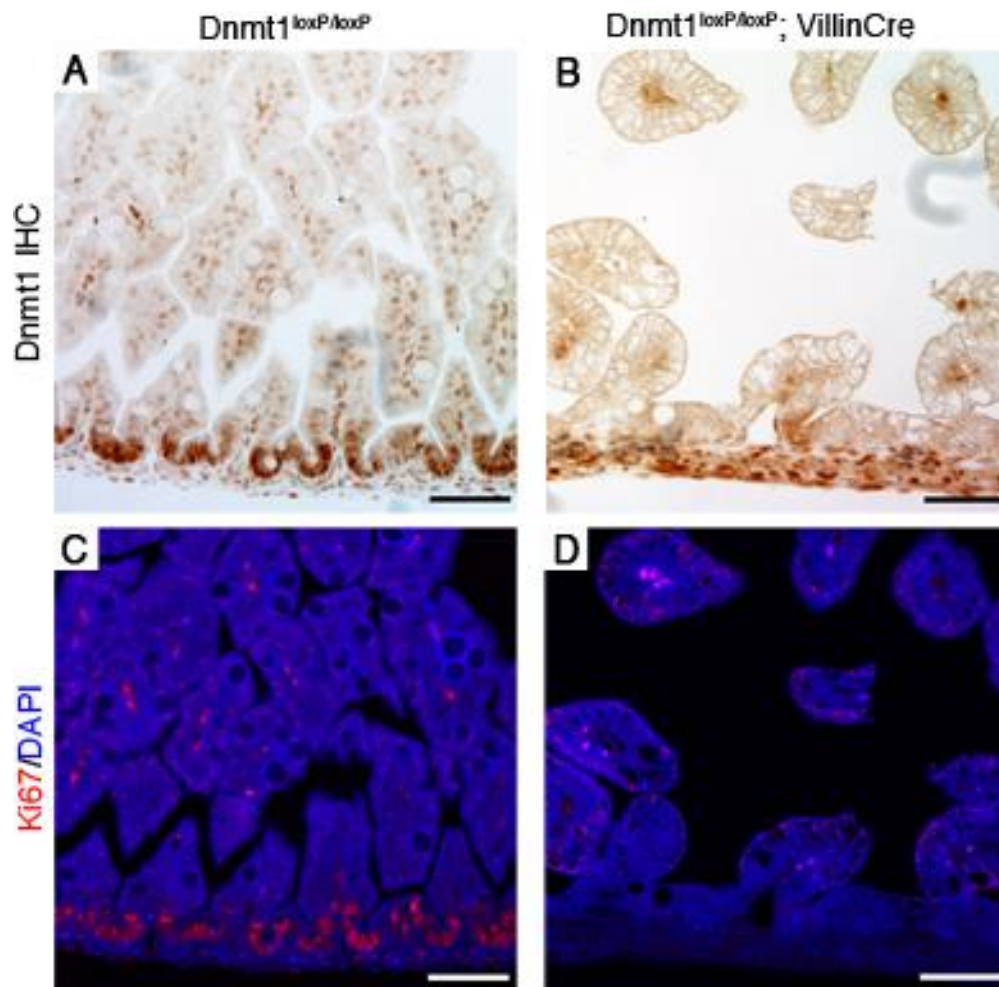
Supplemental Figure S1. *Time course of Dnmt1 localization during intestinal epithelial development. (A-D) Dnmt1 is expressed in the intervillus regions during late fetal development, and becomes restricted to crypts in the adult intestine. Dnmt1 protein stain is brown; hematoxylin nuclear counterstain is blue. Scale bars are 50 μm.*



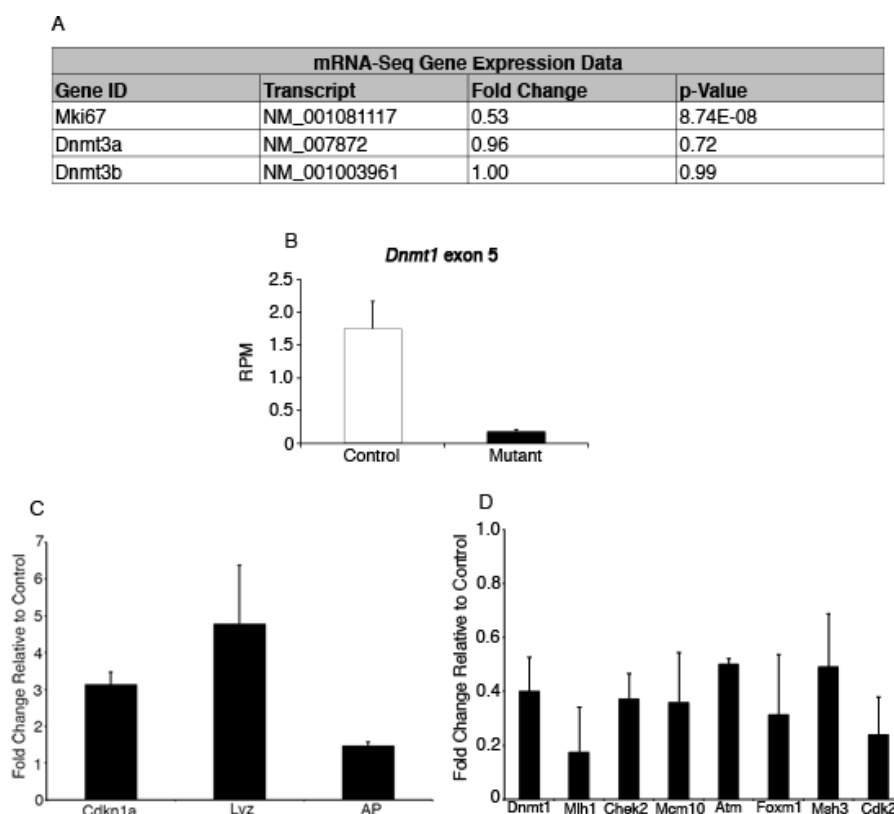
Supplemental Figure S2. Embryonic $Dnmt1^{loxP/loxP}; VillinCre$ intestine is highly mosaic for $Dnmt1$ ablation, while the adult $Dnmt1^{loxP/loxP}; VillinCre$ is repopulated by cells that have escaped Cre-mediated $Dnmt1$ ablation. (A-C) E18.5 mutants showed variable levels of $Dnmt1$ -ablation, with the majority of intervillus regions retaining expression of $Dnmt1$ protein (B,C). (D,E) $Dnmt1$ immunohistochemistry in controls and mutants at 3 months of age revealed that mutant intestines are predominantly $Dnmt1^+$. Scale bars are 50 μm .



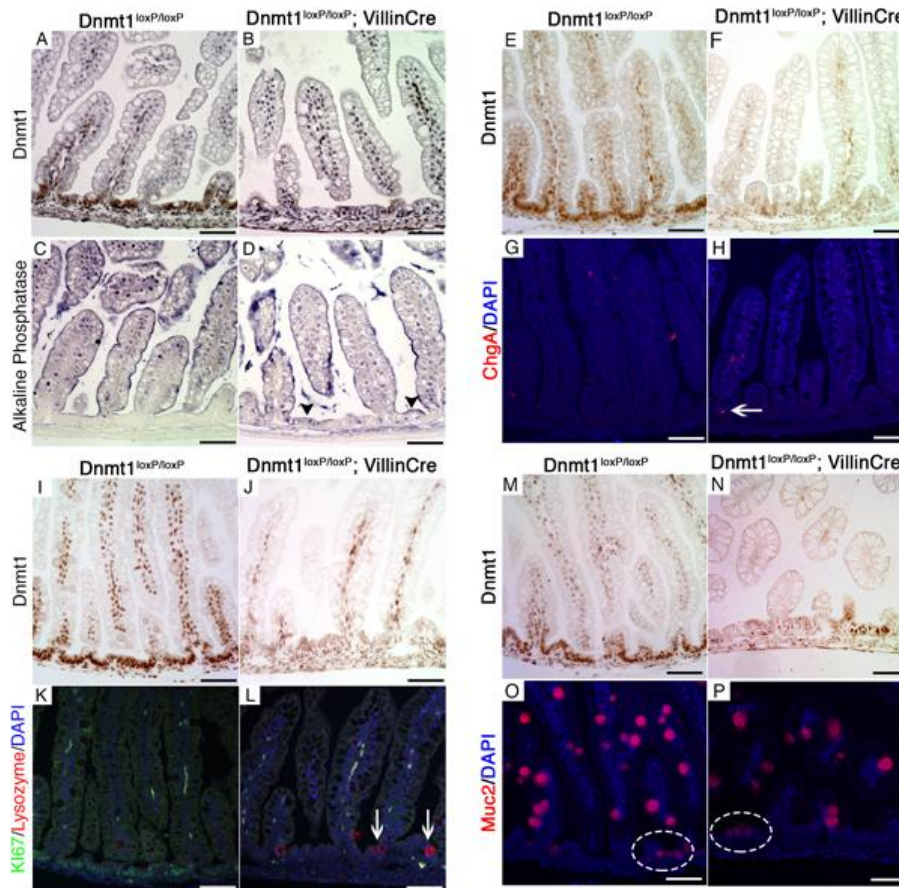
Supplemental Figure S3. *Dnmt3a* and *Dnmt3b* are not upregulated in $Dnmt1^{loxP/loxP}; VillinCre$ neonatal mutants. (A,B) Immunohistochemistry for Dnmt1 in $Dnmt1^{loxP/loxP}$ controls and $Dnmt1^{loxP/loxP}; VillinCre$ mutants. (C) qRT-PCR of whole neonatal proximal jejunum showed a significant decrease in *Dnmt1* transcript in mutants compared to littermate controls. (D-E,G-H) Immunostaining on serial sections demonstrated no change in Dnmt3a (green, second row) and Dnmt3b (red, third row) localization. (F,I) qRT-PCR does not reveal a significant difference in *Dnmt3a* or *Dnmt3b* gene expression. In all images, scale bars are 50 μ m. For all qRT-PCR, control n=10, mutant n=12. Data are represented as mean \pm SEM. (***) $p < 0.001$, two-tailed Student's t-test.



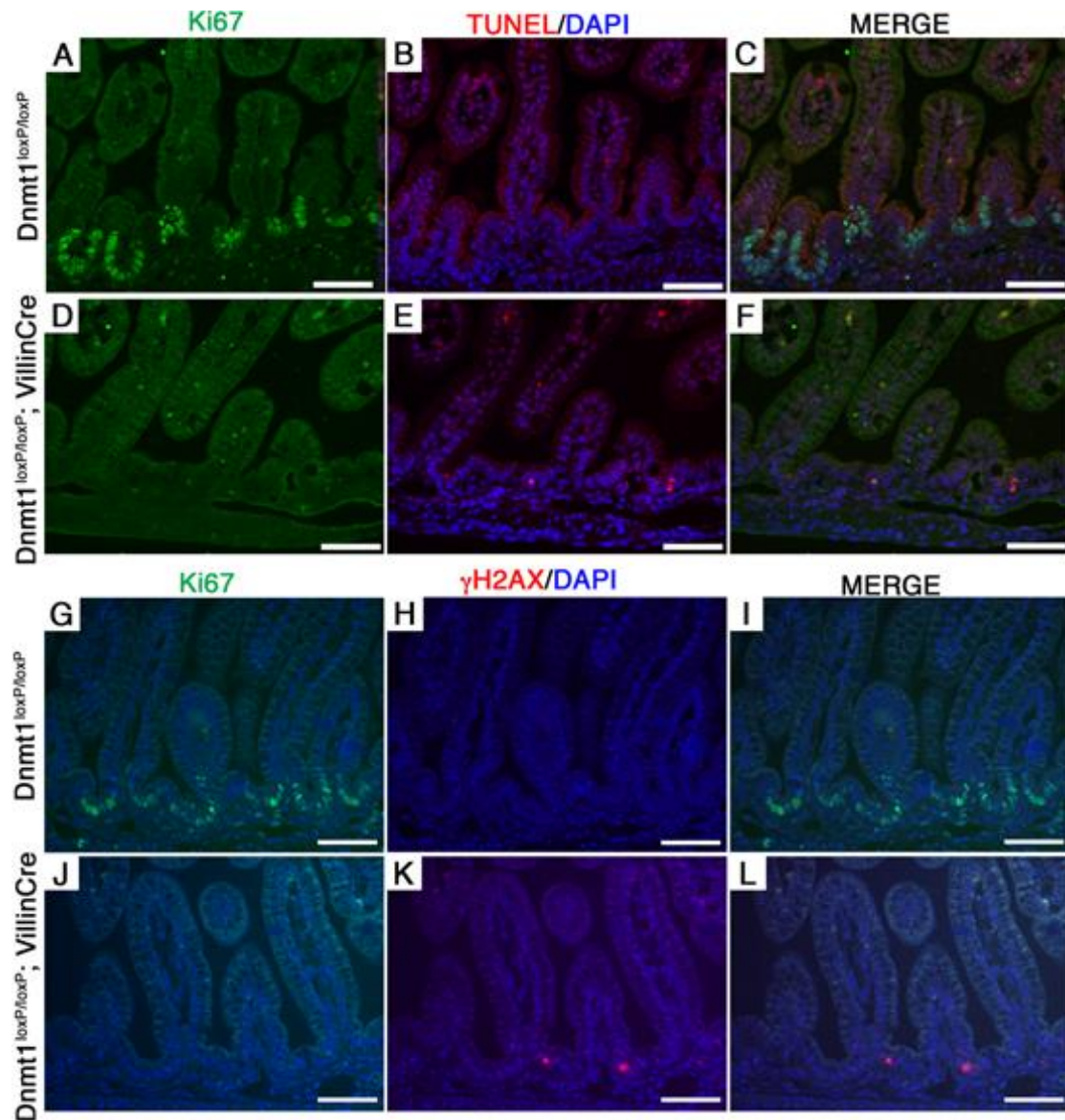
Supplemental Figure S4. *Dnmt1* and *Ki67* protein are co-localized in the intervillus progenitor zone. (A-D) Co-staining for *Dnmt1* (A,B) and *Ki67* (C,D) using separate imaging of each protein on the same section revealed strong overlap of *Dnmt1* and *Ki67* proteins in controls (A,C). *Dnmt1*^{loxP/loxP}; *VillinCre* epithelial cells with *Dnmt1* ablation (B), do not express *Ki67* (D).



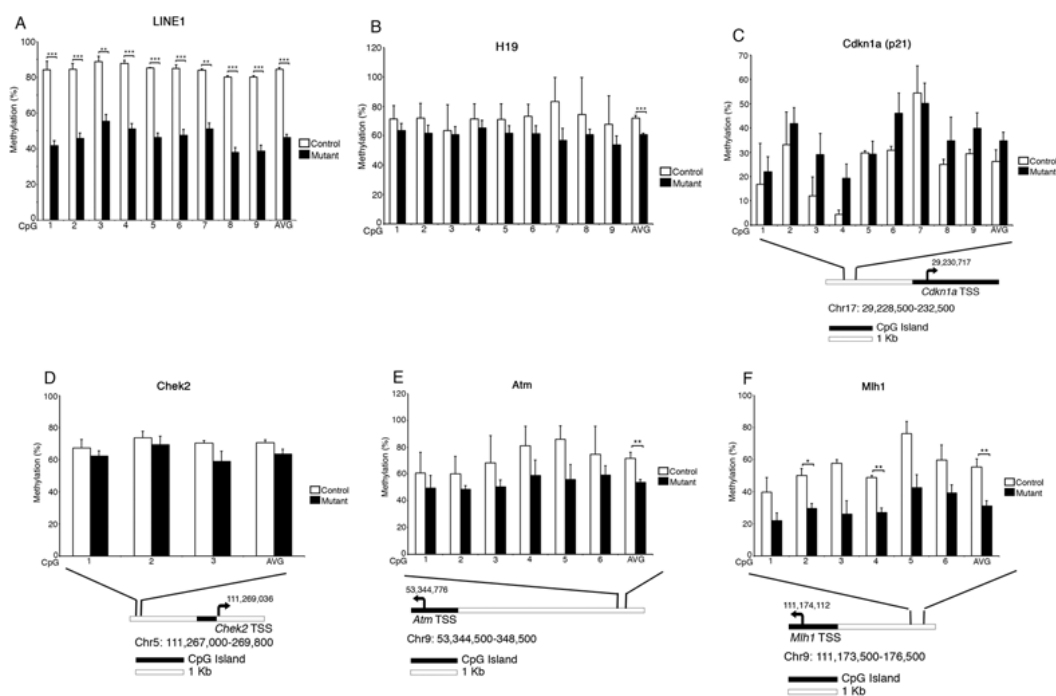
Supplemental Figure S5. Collection of *Dnmt1*-ablated progenitors cells by Laser Capture Microdissection (LCM). (A) Gene expression levels of *Dnmt3a*, *Dnmt3b*, and *mKi67* from RNA-Seq data. Fold change is relative to control. (B) RNA-Seq expression of *Dnmt1* exon 5, which is excised upon Cre activation, indicates a nearly 90% reduction in *Dnmt1* mRNA levels in the LCM tissue of *Dnmt1^{loxP/loxP}; VillinCre* compared to controls (RPM, Reads per Million). (C,D) We performed additional LCM to confirm RNA-Seq data in independent biological replicates (*Dnmt1^{L/L}* controls, n=4; *Dnmt1^{L/L}; VillinCre* mutants, n=3). (C) qRT-PCR confirmation of genes that are misregulated in RNA-Seq data: *Dnmt1*, *Chek2*, *Atm*, *Mcm10*, *Cdk2*, *Mlh1*, *Foxm1*, and *Lyz*. (D) Validation of *p21* (*Cdkn1a*) expression levels, which is upregulated in our RNA-Seq data. qRT-PCR data are presented normalized to the geometric mean of 5 reference genes: *Tbp*, *B2m*, β -actin, *Polr2b*, and *Rplp0*. (B-D) Data are represented as mean \pm SEM. (*) $p < 0.05$, (**) $p < 0.01$, one-tailed Student's t-test.



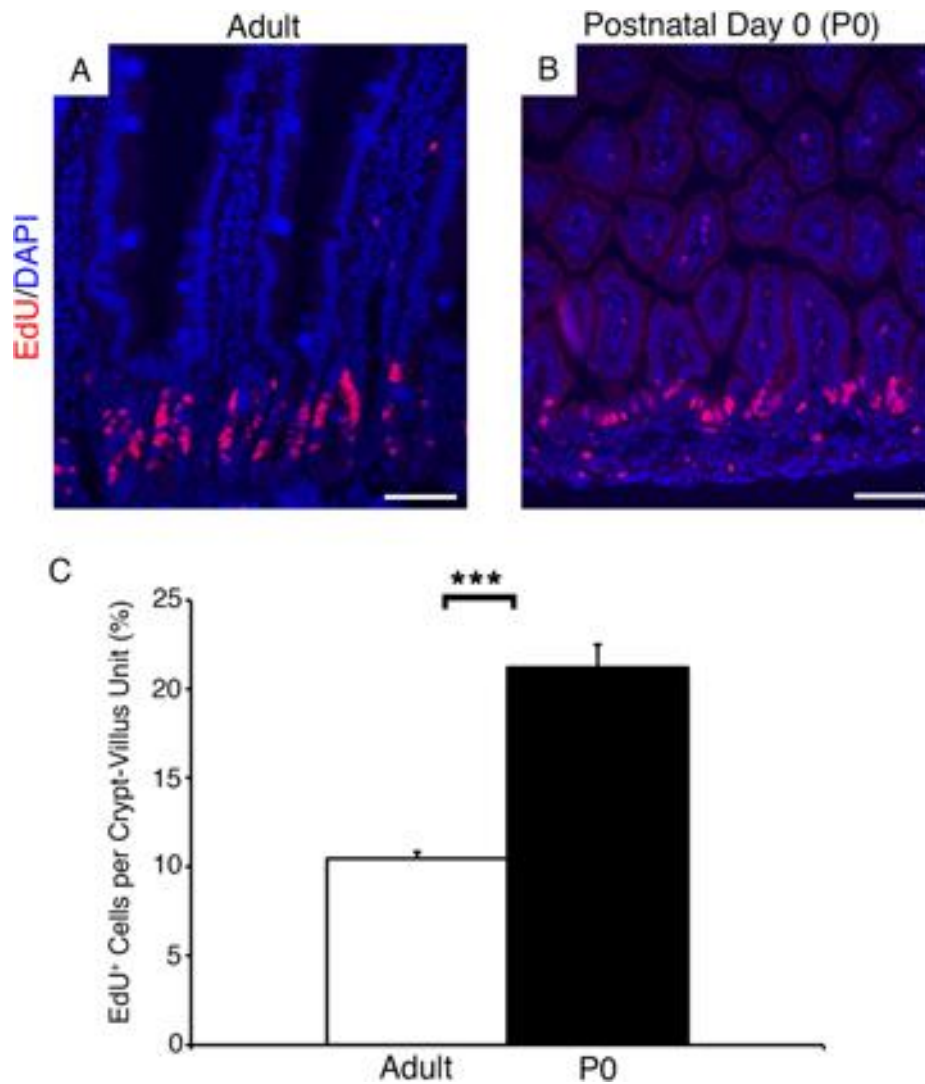
Supplemental Figure S6. Enterocyte, enteroendocrine, Paneth, and goblet cell populations in *Dnmt1^{loxP/loxP}; VillinCre* mutants. (A-B, E-F, I-J, M-N) *Dnmt1* immunohistochemistry on serial sections confirms loss of *Dnmt1* in the mutant regions analyzed. (A-D) Alkaline phosphatase (AP) staining for absorptive enterocytes revealed a small increase in AP⁺ mutant progenitor cells (black arrowheads in D) relative to controls (C). (E-H) Chromogranin A (ChgA) staining for enteroendocrine cells revealed a small increase in ChgA⁺ progenitor cells in mutants (H, white arrow) compared to controls (G). (I-L) Co-staining for Ki67 (green) and lysozyme (red) in control and *Dnmt1* mutant intestine. Non-replicating *Dnmt1*-mutant progenitors had increased lysozyme protein (L, white arrows), a marker for Paneth cell differentiation, relative to controls (K). (M-P) Mucin2 staining showed similar staining patterns of goblet cells in control (O, circled cells) and *Dnmt1* mutant (P, circled cells) progenitor zones. In all images, scale bars are 50 μ m.



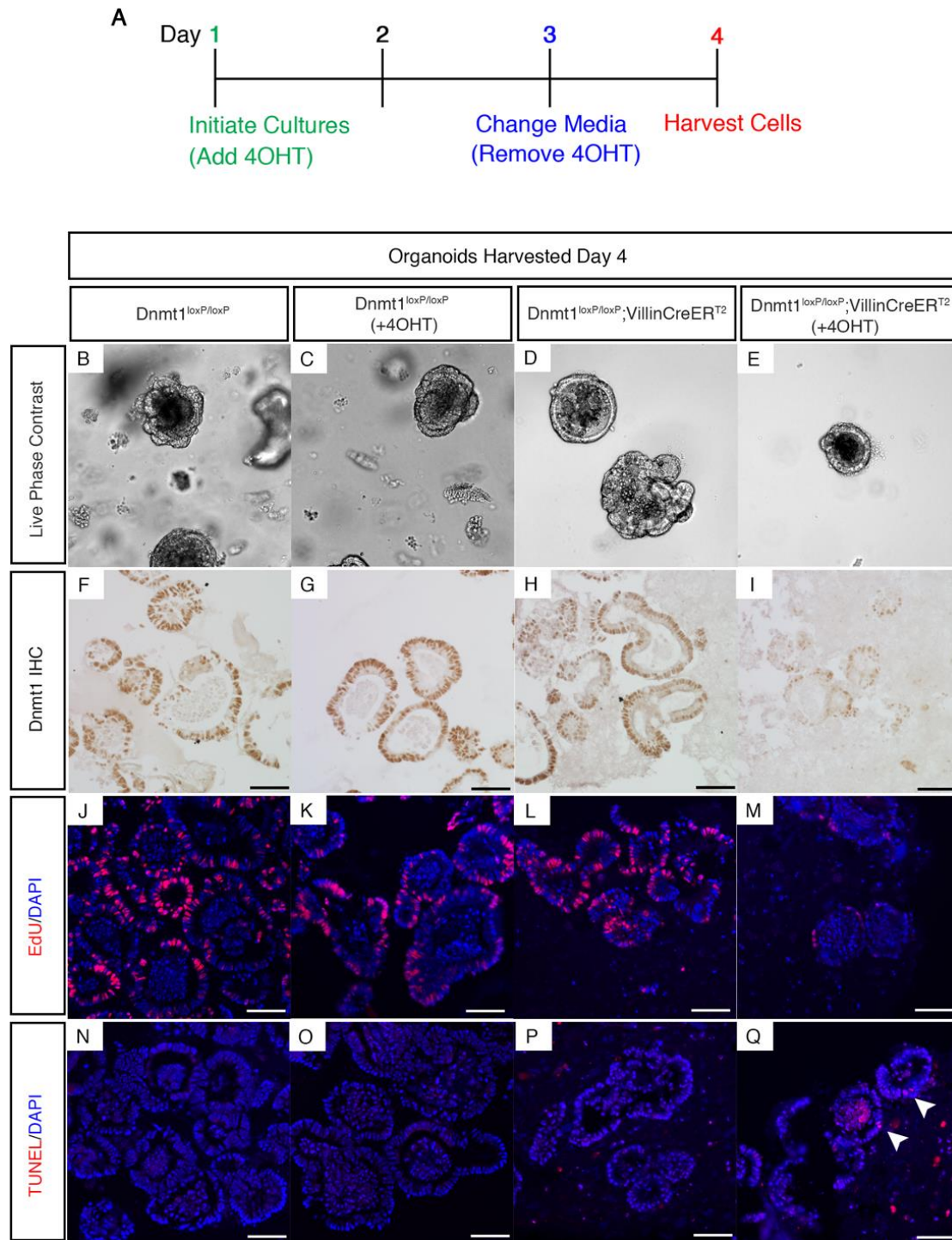
Supplemental Figure S7. *Apoptosis and DNA damage in $Dnmt1^{loxP/loxP}; VillinCre$ mutant mice are confined to the non-replicating intervillus epithelium.* (A-F) Co-staining for Ki67 (green, A,D) with TUNEL (red, B,E) in control (A-C) and $Dnmt1$ -mutants (D-F). Mutant progenitor zones harbor TUNEL⁺ apoptotic cells that correspond with Ki67-negative non-proliferative regions (D-F). (G-M) γ H2AX co-stained with Ki67 revealed that control epithelium does not contain DNA-damaged cells in the progenitor zone (G-I). Ki67-negative, mutant progenitors cells have increased levels of DNA damage (J-L). Scale bars are 50 μ m.



Supplemental Figure S8. *Dnmt1*^{loxP/loxP}; *VillinCreER*^{T2} adult crypt epithelial cells are demethylated at the LINE1 locus, but not at DNA damage response genes. (A) LINE1 repeat DNA methylation levels as assessed by bisulfite-sequencing. Decreased LINE1 methylation suggests global demethylation in *Dnmt1*-ablated adult crypt cells relative to controls. (B) In the H19 imprinting control region (ICR), DNA methylation levels are slightly decreased in adult *Dnmt1*-mutant crypt cells relative to controls. (C-F) Targeted bisulfite-sequencing analysis of DNA damage response genes revealed similar levels of DNA methylation in adult *Dnmt1*-ablated crypt cells compared to controls. (C,D) *Cdkn1a* (*p21*) and *Chek2* are not differentially methylated in adult *Dnmt1*-mutant crypts. *Atm* (E) and *Mlh1* (F) show an overall decrease in DNA methylation relative to control, but are not significantly altered at each CpG analyzed. Below (C-F) are diagrams indicating the relative position of the transcription start site (TSS, black arrow) and CpG islands compared to the locations sequenced. Each region is approximately 2-4 kb upstream of the TSS. Mutant n=5; Control n=2. (**) $p < 0.01$, (***) $p < 0.001$, two-tailed Student's t-test.

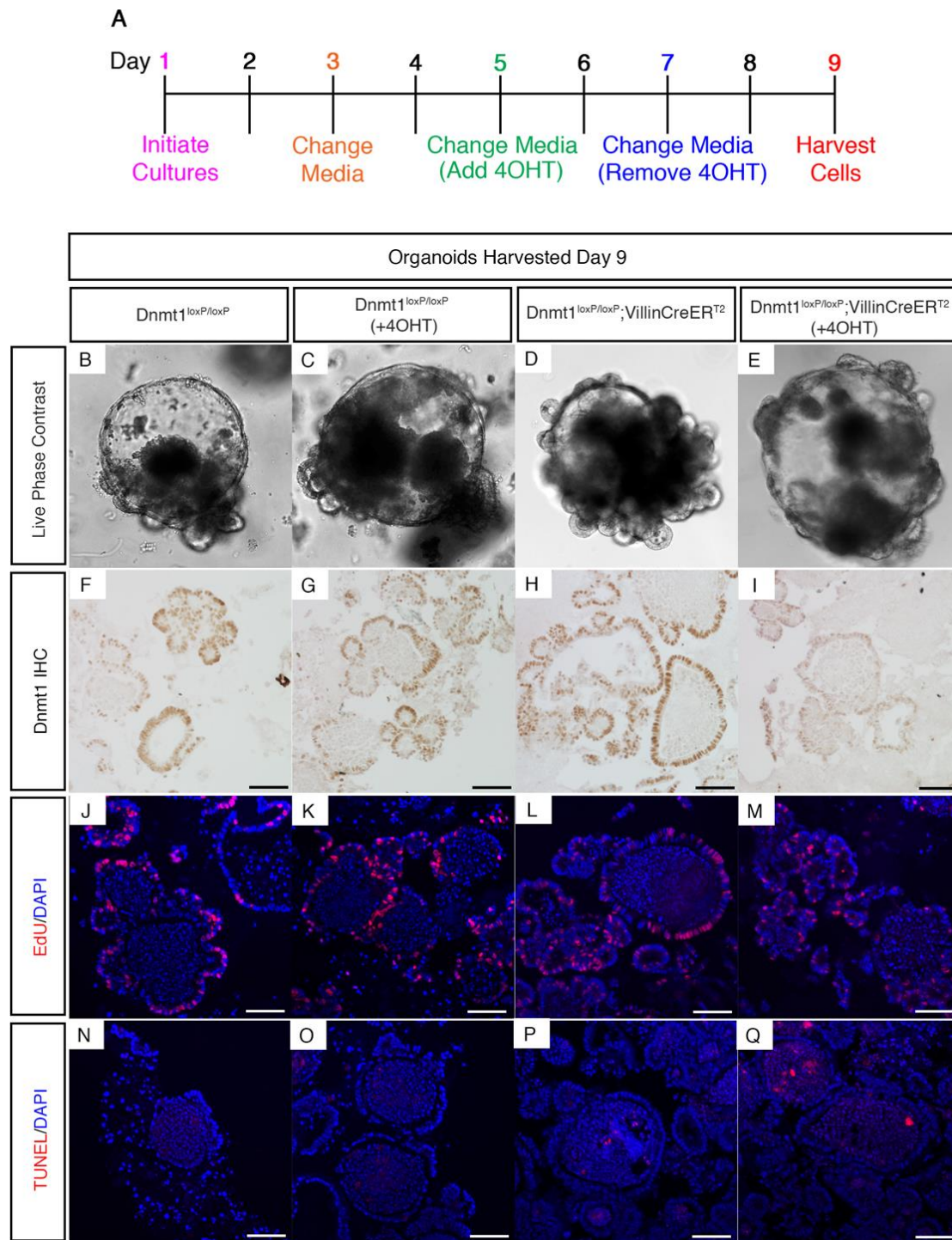


Supplemental Figure S9. Neonatal intervillus regions display increased rate of replication compared to adult crypts. (A,B) Representative images of adult (A, n=5) and postnatal day 0 (B, n=12) jejunum stain for EdU following a 2-hour EdU pulse (red). (C) Percent of EdU⁺ cells per crypt-villus subunit is approximately two-fold higher in the neonatal compared to the adult jejunum. Rates calculated as percent EdU⁺ nuclei of total nuclei between two adjacent villi peaks. Scale bars are 50 μ m. Data are represented as mean \pm SEM. (***) $p < 0.001$, two-tailed Student's t-test.



Supplemental Figure S10. *Dnmt1* is required to establish intestinal organoid cultures. (A) Time course of 4OHT treatment in organoids from $Dnmt1^{loxP/loxP}$ and $Dnmt1^{loxP/loxP}; VillinCreER^{T2}$ adult intestine to test the requirement for *Dnmt1* in establishment of intestinal crypts *in vitro*. (B-Q) Immunohistochemical analysis of

organoids described in (A). (B-E) Live phase contrast imaging demonstrates reduced size and budding activity of *Dnmt1*-ablated organoids (E) compared to controls (B-D). All phase contrast images were captured at 10X. (F-I) Dnmt1 protein is reduced in *Dnmt1^{loxp/loxp}; VillinCreER^{T2}* organoids upon treatment with 4OHT (I), relative to control organoids (F-G). (J-M) 2 hour EdU treatment shows reduced replication rate of *Dnmt1*-mutant organoids (M) compared to controls (J-L). (N-Q) *Dnmt1*-ablated organoids (Q) display increased apoptosis (white arrowheads) relative to non-treated controls (N,P). Additionally, apoptosis is not increased in control *Dnmt1^{loxp/loxp}* organoids treated with 4OHT (O). All scale bars are 50 μ m.



Supplemental Figure S11. *Dnmt1* is not necessary to maintain established intestinal organoid cultures. (A) Time course of 4OHT treatment to test requirement for *Dnmt1* in maintenance of intestinal crypts *in vitro*. (B-Q) Immunohistochemical analysis of organoids described in (A). (B-E) Live phase contrast imaging demonstrates similar size of *Dnmt1*-ablated organoids (E) at day 9 of culture relative to 4OHT-treated (C)

and non-treated (*B,D*) controls. All phase contrast images were captured at 10X. (*F-I*) Confirmation of Dnmt1 protein depletion in 4OHT-treated *Dnmt1^{loxp/loxp}; VillinCreER^{T2}* organoids (*I*) compared to controls (*F-H*). (*J-M*) A 2-hour pulse of EdU reveals preserved replication of *Dnmt1*-mutant organoids (*M*), similar to that observed in control organoids (*J-L*). (*E,I*) *Dnmt1*-ablated organoids do not display any changes in apoptosis (*Q*) compared to treated (*O*) or non-treated (*N,P*) control organoids. TUNEL positive material in (*P,Q*) is typical debris accumulation within organoids. All scale bars are 50 μ m.

Table S1

[Click here to Download Table S1](#)

Table S2

[Click here to Download Table S2](#)